The Orinoco Low-Level Jet and Its Association with the Hydroclimatology of Northern South America

ALEJANDRO BUILES-JARAMILLO,[a] JOHANNA YEPES,[a] AND HERNÁN D. SALAS[a]

[a] *Facultad de Arquitectura e Ingeniería, Institución Universitaria Colegio Mayor de Antioquia, Medellín, Colombia*

(Manuscript received 13 April 2021, in final form 21 October 2021)

ABSTRACT: We investigated the relationship between the frequency of occurrence of the Orinoco low-level jet (OLLJ) and hydroclimatic variables over northern South America. We use data from the ERA5 atmospheric reanalysis to characterize the spatial and temporal variability of the OLLJ in light of the low-level jet (LLJ) classification criteria available in the literature. An index for the frequency of occurrence of an LLJ was used, based on the hourly maxima of wind speed. The linkages among the OLLJ, water vapor flux, and precipitation were analyzed using a composite analysis. Our results show that during December–February (DJF), the OLLJ exhibits its maximum wind speed, with values around 8–10 m s^{-1}. During DJF, the analysis shows how the OLLJ transports atmospheric moisture from the tropical North Atlantic Ocean. During this season, the predominant pathway of the OLLJ is associated with an area of moisture flux divergence located over northeastern South America. During June–August (JJA), an area of moisture flux convergence associated with the northernmost location of the ITCZ inhibits the entrance of moisture from northerlies. We also show that the occurrence of the OLLJ is associated with the so-called cross-equatorial flow. During DJF, the period of strongest activity of the OLLJ is associated with the northerly cross-equatorial flow and dry season, whereas during JJA the southerly cross-equatorial flow from the Amazon River basin predominates and contributes to the rainy season over the Orinoco region.

KEYWORDS: Atmosphere; South America; Jets; Climatology; Seasonal variability

1. Introduction

Low-level jets (LLJs) are important mechanisms for transporting atmospheric moisture. They modulate both the weather and the climate (Bonner 1968; Stensrud 1996; Walters et al. 2014; Gimeno et al. 2016). Some LLJs have great climatic importance, such as the Great Plains low-level jet (GPLLJ), Gulf of California low-level jet (GCLLJ), Caribbean low-level jet (CLLJ), Choco low-level jet (ChocoJet), South American low-level jet (SALLJ), Turkana low-level jet (Turkana LLJ), Somali low-level jet (Somali LLJ), Koorin low-level jet, and southerly buster (Bonner 1968; Findlater 1969; Kinuthia and Asnani 1982; Brook 1985; Douglas 1995; Amador 1999; Poveda and Mesa 2000; Vera et al. 2006; Wang 2007; Gimeno et al. 2016). Over northern South America, the CLLJ, the ChocoJet, the SALLJ, and the Orinoco LLJ are prominent features that modulate the climate of the region (Wang 2007; Muñoz et al. 2008; Whyte et al. 2008; Martin and Schumacher 2011; Poveda and Mesa 2000; Yepes et al. 2019; Vera et al. 2006; Montini et al. 2019; Gimeno et al. 2016; Montoya et al. 2001).

Low-level jets are traditionally defined based on the relative maximum in the vertical profile of the horizontal wind speed. Bonner (1968) proposed a hierarchy of criteria based on wind speed for the classification of the GPLLJ. These criteria evaluate the gradient between the maximum wind speed at the LLJ core and the wind speed at the upper and lower levels of that wind maximum. There is extensive use of these criteria for other jets in the world, although they are limited by the wind speed thresholds, which avoid identifying other LLJ with lower wind speeds. Hence, some works have developed other criteria to evaluate LLJ activity (Whiteman et al. 1997; Rife et al. 2010; Ranjha et al. 2013). In particular, Ranjha et al. (2013) focus on coastal LLJs and include temperature and wind speed variations in the criteria, developing a frequency indicator of occurrence. These modifications include a set of criteria that can be used systematically to scan global datasets for identifying the locations and occurrences based on the vertical profiles of the wind speed and temperature at coastal areas.

The northernmost continental territory of Colombia is affected by winds of the CLLJ, whereas its western Pacific coast, in the far-eastern tropical Pacific Ocean, is affected by the ChocoJet (Poveda and Mesa 2000; Morales et al. 2017; Arias et al. 2015; Yepes et al. 2019). Additionally, there is evidence of a low-level jet located at the east of the Andean territory of Colombia and Venezuela, known by several names: the Eastern Andean LLJ or Corriente de Los Andes Orientales (CAO, in Spanish) (Montoya et al. 2001; Torrealba and Amador 2010), Llanos LLJ (LaBar et al. 2005; Rueda 2014), and Orinoco LLJ (OLLJ; Jiménez-Sánchez et al. 2019).

The OLLJ has been studied at different time scales. Seasonally, Montoya et al. (2001) reported the low-level winds over eastern Colombia and found, using NCEP–NCAR reanalysis, that the OLLJ was predominantly a December–February (DJF) atmospheric feature. They proposed that the OLLJ may originate from the flow generated by the interaction between the westernmost extension of the North Atlantic Subtropical High (NASH) and an anomalous low pressure over South America during DJF. Furthermore, Rueda (2014) characterized the OLLJ using the ERA-Interim reanalysis and confirmed that the jet is stronger during the dry season in the eastern Colombian region (DJF), with a core between 1000 and 850 hPa and mean wind speed around 6–8 m s^{-1}. Also, the OLLJ is a mechanism

Corresponding author: Alejandro Builes-Jaramillo, luis.builes@colmayor.edu.co

DOI: 10.1175/JHM-D-21-0073.1

for transporting pollutants across the Orinoco basin toward Ecuador during the fire season in northern South America (February–April) (Rodríguez-Gómez et al. 2022).

At diurnal scales, Torrealba and Amador (2010) characterized the OLLJ using pilot balloons and radiosondes. They found the highest wind speeds at 1200 UTC (0700 LST) with values around 14 m s^{-1} during January–February in the period 2001–07 over the center of the Venezuelan plains. Recently, Jiménez-Sánchez et al. (2020) modeled the characteristics and evolution of the OLLJ using dynamical downscaling performed in a 5-month-long simulation from November 2013 to March 2014. Following the methods established by Bonner (1968) and Ranjha et al. (2013), they identified an 89% frequency of occurrence of the OLLJ during the period of analysis. They also distinguished four main cores along the OLLJ pathway, each constrained by topographic effects. Their numerical simulation experiment revealed that the maximum diurnal mean wind speeds (13–17 m s^{-1}) occur at each core location, at a different time during the night and early morning (0300–1400 UTC). According to Jiménez-Sánchez et al. (2020), the OLLJ is the result of four dynamical processes: a sea breeze penetration, katabatic flow, three expansion fans, and diurnal variation of turbulent diffusivity. These processes act together to maintain the acceleration of the winds in the LLJ corridor.

Over the Orinoco plains shared by Colombia and Venezuela, precipitation exhibits a unimodal annual cycle with a dry season during DJF and a wet season during June–August (JJA) (Urrea et al. 2019). In terms of the effects of the OLLJ on the precipitation over the region, LaBar et al. (2005) studied the influence of the OLLJ on convective precipitation over the Venezuelan plains and found that the OLLJ winds are the strongest in the dry season (DJF) at 925 hPa and the weakest in the wet season (JJA). Moreover, LaBar et al. (2005) showed that during the dry season, deep convection is practically nonexistent across the midcorridor of the jet (Venezuela) but indeed occurs to the south, around the exit region of the OLLJ (southern Colombia). Nevertheless, the relationship between the moisture pathways through LLJs (Algarra et al. 2019) and precipitation in the region needs further analysis.

The present study aims to investigate the seasonal variability of the OLLJ and its relation to hydroclimatic variables in the region using the ERA5 reanalysis (Hersbach et al. 2019) and Climate Hazards Group Infrared Precipitation with Station data (CHIRPS) database (Funk et al. 2015). Our interest focuses on the seasons of extreme activity of the OLLJ and their influence over the dry (wet) seasons in northern South America. Bearing in mind that Jiménez-Sánchez et al. (2019) and Jiménez-Sánchez et al. (2020) analyzed a 5-month simulation, and that there are few works that have studied the OLLJ in association with precipitation, we address the following questions:

1) What is the annual cycle of the OLLJ according to ERA5?
2) How is the OLLJ related to moisture transport during the wet season?
3) How is OLLJ activity related to precipitation variability on day-to-day and seasonal time scales?

This paper is organized as follows. Section 2 describes the regions of study and general information about the datasets used. Section 3 gives a brief description of the frequency of occurrence of LLJs, as well as the procedure to quantify the associations between precipitation and the OLLJ. The results and a discussion are presented in section 4, and conclusions are drawn in section 5.

2. Data

a. Reanalysis

We use data from the ERA5 atmospheric reanalysis (Hersbach et al. 2019), which provide estimates of atmospheric, land, oceanic, and climatic variables. The ERA5 data cover Earth with a 30 km grid having 137 levels, from the surface up to a height of 80 km. Here, we use the following variables: daily and hourly zonal and meridional wind speeds at pressure levels from 1000 to 500 hPa, vertically integrated moisture divergence flux, specific humidity, omega at 500 hPa, and the zonal and meridional and vertically integrated water vapor fluxes (northward/eastward). We also estimated the total precipitable water (TPW) from ERA5 data using

$$\mathrm{TPW} = \frac{1}{\rho g}\int_{p_{\mathrm{sup}}}^{p_{\mathrm{top}}} q(p)dp,$$

where ρ represents the density of water, g is the acceleration due to gravity, and q is the specific humidity integrated from the surface to the top of the atmosphere. The region of interest is 10°S–20°N and 85°–50°W, and the period of study is 1981–2019.

b. Precipitation

We use data from CHIRPS, which is a high-resolution dataset (0.25°), at daily and monthly time scales in the quasi-global rainfall dataset from 1981 to near-present (Funk et al. 2015). In this work, we use a spatial resolution of 0.25° and a daily time resolution from 1 January 1981 to 31 December 2019 over northern South America (10°S–20°N and 85°–50°W). We also used data from the Global Precipitation Climatology Centre (GPCC) Full Data Reanalysis version 7 gridded at a resolution of 0.5° × 0.5° (Schneider et al. 2014).

Six rain gauge stations were used to compute an ensemble of the annual cycle of precipitation over the Orinoco region in Colombia (Table 1 and Fig. 1). All of these stations have continuous records of more than 20 years and with no more than 5% missing data. The rain gauge data can be obtained directly from the Colombian Institute for Environmental Studies (IDEAM) at the Hydrological and Meteorological data management website (http://dhime.ideam.gov.co).

3. Methods

a. Estimation of the frequency of occurrence of an LLJ

We use the criteria proposed by Jiménez-Sánchez et al. (2019) to identify the frequency of occurrence of the OLLJ.

TABLE 1. Precipitation measuring stations and datasets in the Orinoco region.

Station/dataset	Location	Period
Chaparrera	5.49°N, 72.22°W	1995–2020
Huerta	4.65°N, 72.91°W	1995–2020
Macucuana	4.90°N, 71.53°W	1983–2019
Matezamuro	6.97°N, 70.85°W	1983–2019
Molinos	5.41°N, 72.29°W	1995–2019
Palenque	5.42°N, 71.72°W	1974–2019
CHIRPS	2°N, 74°W; 7°N, 68°W	1981–2019
GPCC	2°N, 74°W; 7°N, 68°W	1982–2016

These criteria are based on both Bonner (1968) and Ranjha et al. (2013), as follows:

- The level of maximum wind is within the lowest 2 km above ground level.
- The wind speed at the level of maximum wind is at least 40% higher than the wind speed at the surface (i.e., the lowest model level, 1000 hPa).
- The wind speed above the level of maximum wind decreases by at least 20% within 3 km of the surface.

We computed the wind speed for the study region, and we tested these three conditions: grid cells that match the three conditions were flagged as 1, otherwise were flagged as 0. This calculation was done for hourly instantaneous wind fields from 1981 to 2019 for the months under study at 6-h time intervals according to synoptic times 0000 UTC (1900 LST), 0600 UTC (0100 LST), 1200 UTC (0700 LST), and 1800 UTC (1300 LST). There are two time zones in the region, UTC − 4 and UTC − 5; we selected UTC − 5 as the reference time zone for our study. Once the frequency of the OLLJ was computed in each grid cell, the total days of occurrence was divided by the total number of days. This calculation produces an indicator of the frequency of occurrence of an LLJ that ranges from 0% to 100%.

b. *Composite analysis*

Composite analysis is a well-known method to study the relationships between different climate phenomena (Terray et al. 2003; Boschat et al. 2016; Xie et al. 2017). In general, according to Xie et al. (2017), a composite analysis to infer the association between an index I and a field variable F can be summarized as follows: 1) we define some events or data points using criteria based on the index I; 2) the timings of these events or data points constitute the key times; 3) we isolate the signal in the variable F corresponding to I by calculating the average of F over all key times; and finally, 4) we use statistical tests to verify whether there is a significant difference between the average of F over all key times and the overall average of F (Terray et al. 2003; Boschat et al. 2016).

For the composite analysis, we estimated the extreme events of daily zonal wind speed at 925 hPa. To this end, we selected the time series of this variable over the LLJ index area (6°–8°N and 67°–69°W) (see Fig. 1). Then, these time series were averaged over that area, resulting in a

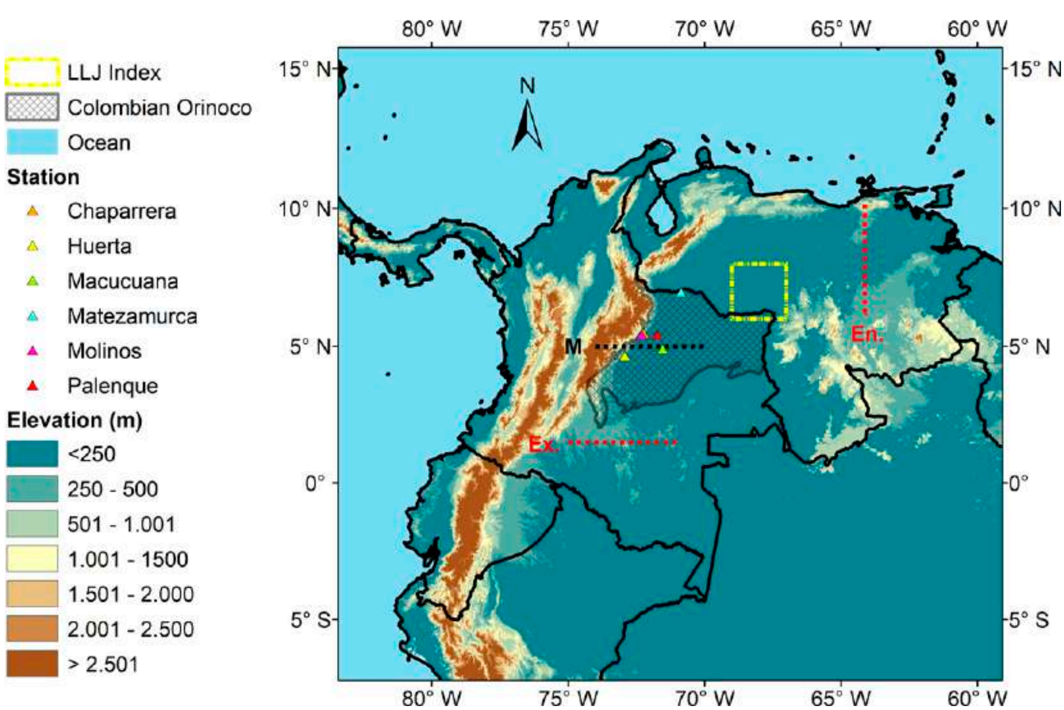

FIG. 1. Region of study and particular areas used to compute annual cycles and indexes, including the Colombian Orinoco, rain gauge stations, and the LLJ index area in the left panel. The dotted lines depict the entrance (En.), mid (M), and exit (Ex.) regions of the OLLJ corridor.

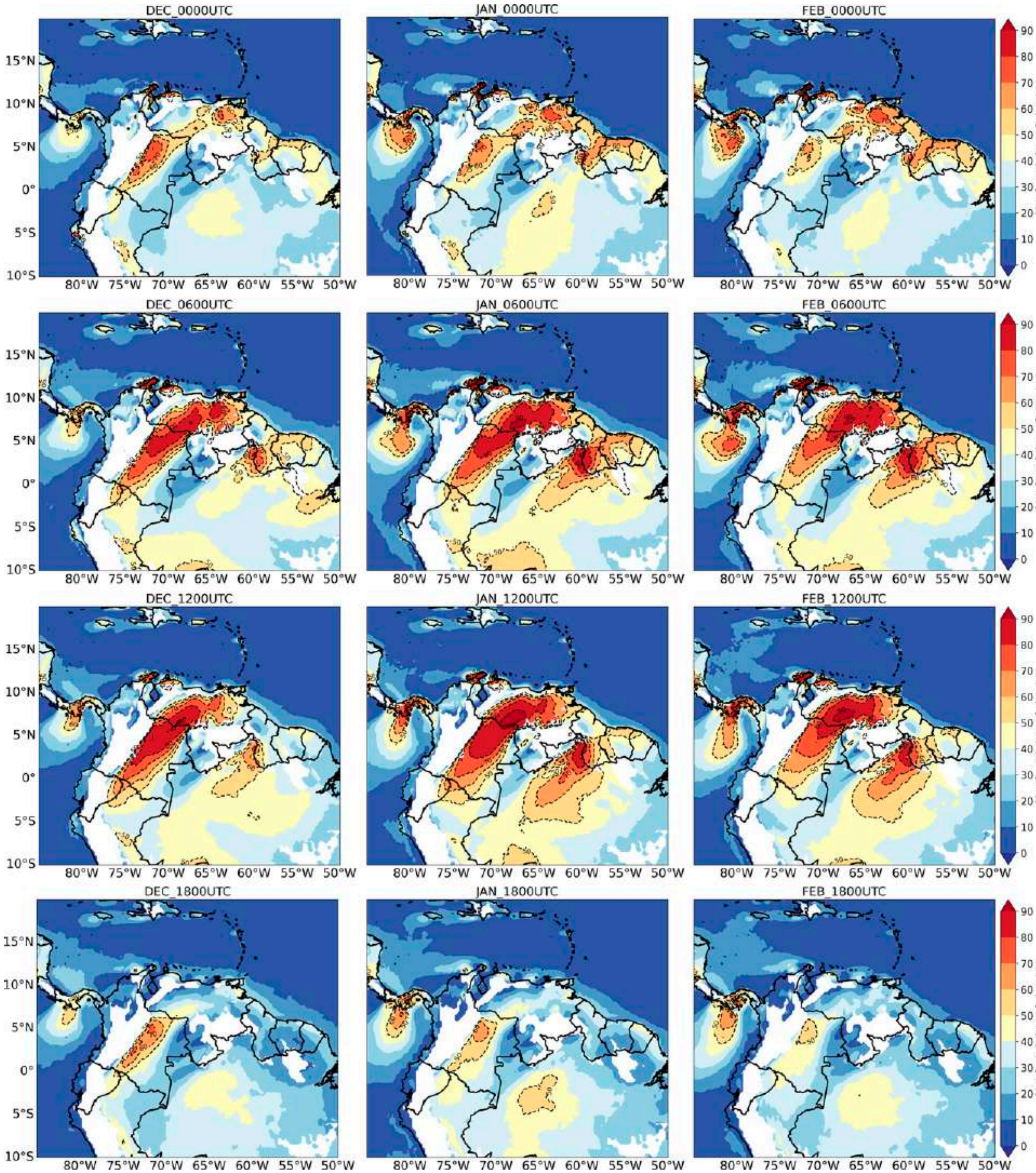

FIG. 2. Monthly percentage of days during the month when the three OLLJ criteria are satisfied during the 1981–2019 period at synoptical hours [0000 UTC (1900 LST), 0600 UTC (0100 LST), 1200 UTC (0700 LST), and 1800 UTC (1300 LST)].

single time series. Subsequently, we used one standard deviation below (above) the mean wind speed to identify strong (weak) events of frequency of the OLLJ during DJF (JJA). Therefore, days with zonal wind speeds below (above) one standard deviation were included in the composite analysis. During these extreme event days, we compute the average daily values for hydroclimatic variables, such as precipitation, zonal and meridional winds, as well as zonal and meridional water vapor flux (Peixoto and Oort 1993). Finally, we verify the statistical significance of the composite fields in relation to the climatology using the statistical test proposed by Terray et al. (2003), which is a

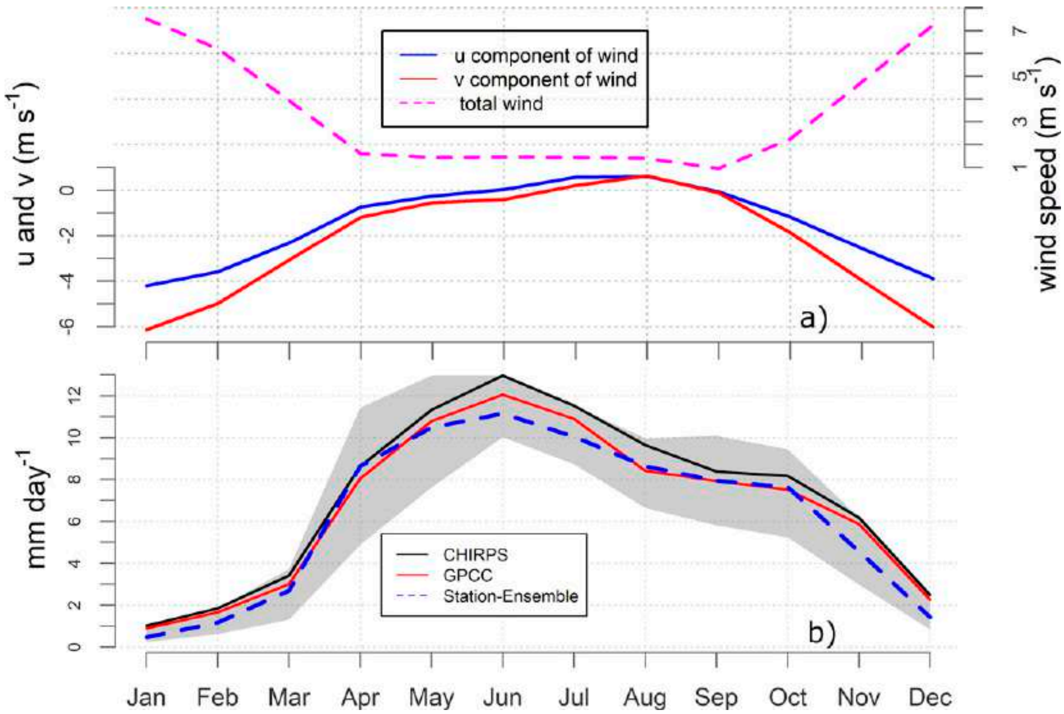

FIG. 3. Annual cycles of (a) wind speeds and (b) precipitation for different datasets. Both annual cycles were estimated over the Colombian Orinoco region indicated in Fig. 1. The gray area in (b) depicts the variance of the stations used to compute the ensemble.

nonparametric procedure to test the hypothesis of equal population means, based on two random samples without prior assumptions such as that the samples belong to normal populations with a common variance but possibly different means. This test can be carried out using simulation, bootstrapping techniques, or randomization tests. In this work, we use bootstrapping to apply Terray et al.'s test. Hereafter, we show the average wind vectors over the statistically significant regions in the composite maps.

The LLJ index area exhibits a mean zonal wind speed of -3.7 m s^{-1}, as well as a standard deviation of 3.5 m s^{-1}. Then, during DJF (JJA), which are the seasons of strong (weak) OLLJ activity (see section 4), we consider the events below (above) one standard deviation from the mean wind speed: zonal wind speeds greater than -7.2 m s^{-1} are considered as the strongest activity events during DJF; daily westerly wind speeds higher than -0.2 m s^{-1} are considered as the weakest activity events during JJA. Dates for these events constitute the key times for the composite analysis, which will be described next.

4. Results

a. Frequency of occurrence of the OLLJ

Figure 2 presents the long-term relative frequency of occurrence of the OLLJ during DJF by month and as a function of the time of day. During DJF, our results show the highest OLLJ frequencies occur at 0600 and 1200 UTC (0100 and 0700 LST) and the lowest at 1800 and 0000 UTC (1300 and 1900 LST). This result agrees with previous studies that have classified the OLLJ as a nocturnal jet (Gimeno et al. 2016; Ranjha et al. 2013; Jiménez-Sánchez et al. 2019; Algarra et al. 2019). At 0000 UTC (Fig. 2, top), frequencies of occurrence above 70% are located over the Venezuela and Guianas coast, the OLLJ midcorridor, and the Panama gap flow. At 1800 UTC (Fig. 2, bottom), values between 40% and 60% are located over the mid and exit regions of the OLLJ and the Panama gap flow. At 0600 and 1200 UTC, the frequency of occurrence of the OLLJ reaches values up to 90% in central Venezuela and eastern Colombia. This region coincides with the maximal wind speeds in Fig. 4. However, another region of high frequency of occurrence, up to 80% (deserving further research), is located between Guiana and Brazil. This region is associated with the Guianas LLJ (Gimeno et al. 2016; Algarra et al. 2019) and could be related to a nighttime acceleration due to a decoupling of the boundary layer as described for the OLLJ by Jiménez-Sánchez et al. (2020) and by the orographic effect by the Guianas shield as shown in Fig. 2.

For December, at 1200 UTC (the hour with the highest frequencies of occurrence), the core of high frequency (80%–90%) of the OLLJ is located in a region that spans a large area from central Venezuela to central Colombia. For January, the core of high frequencies becomes smaller, and the highest frequencies (90%) are mostly located in Venezuela. In February, this region of higher OLLJ activity retreats further over central Venezuela, decreasing its extent over Colombia. In contrast, frequencies of occur-

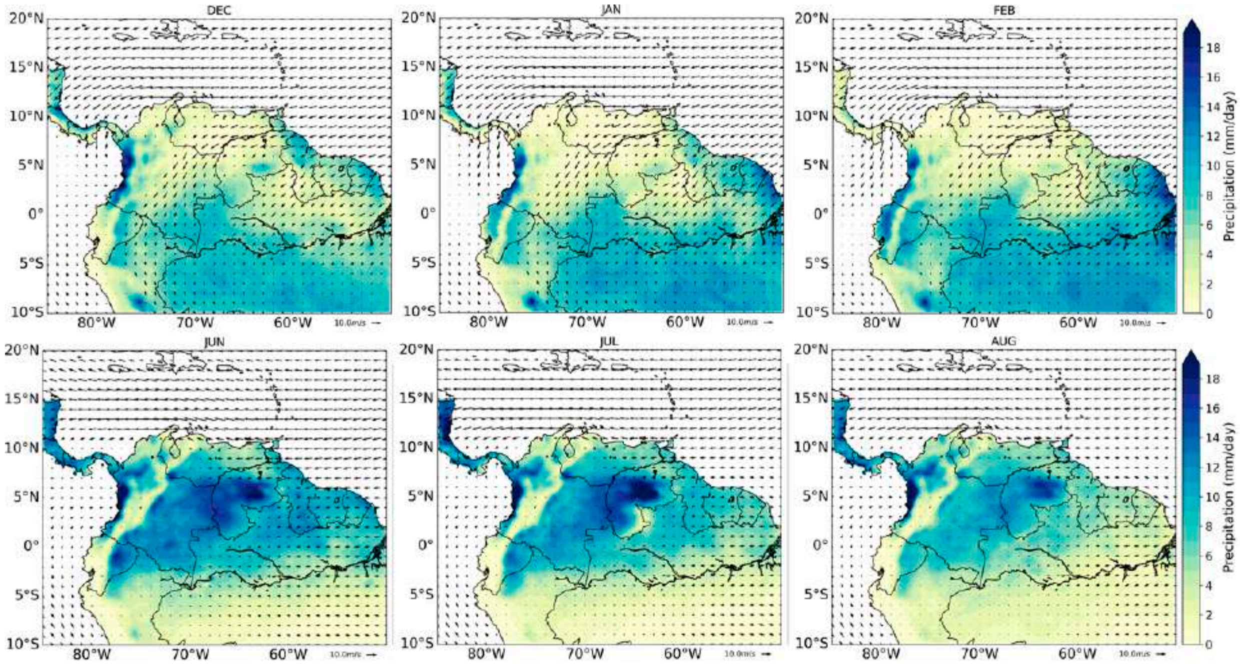

FIG. 4. Long-term mean precipitation (mm day^{-1}) and wind vectors (m s^{-1}) at 925 hPa during December, January, and February (period of the strongest winds of the OLLJ) and June, July, and August (period of its weakest winds). Precipitation and wind data are retrieved from CHIRPS (mm day^{-1}) and ERA5 reanalysis (m s^{-1}) for the period 1981–2019, respectively.

rence tend to increase from December to February for the Guianas LLJ.

The activity criteria show the evolution of the frequency of occurrence of the OLLJ and other low-level flows over the region (contours above 50%) during DJF. The frequency of occurrence also allowed us to pinpoint the Panama gap flow (Xie et al. 2005), which extends to the offshore Colombian Pacific and a high-frequency region over portions of the Guianas and a small

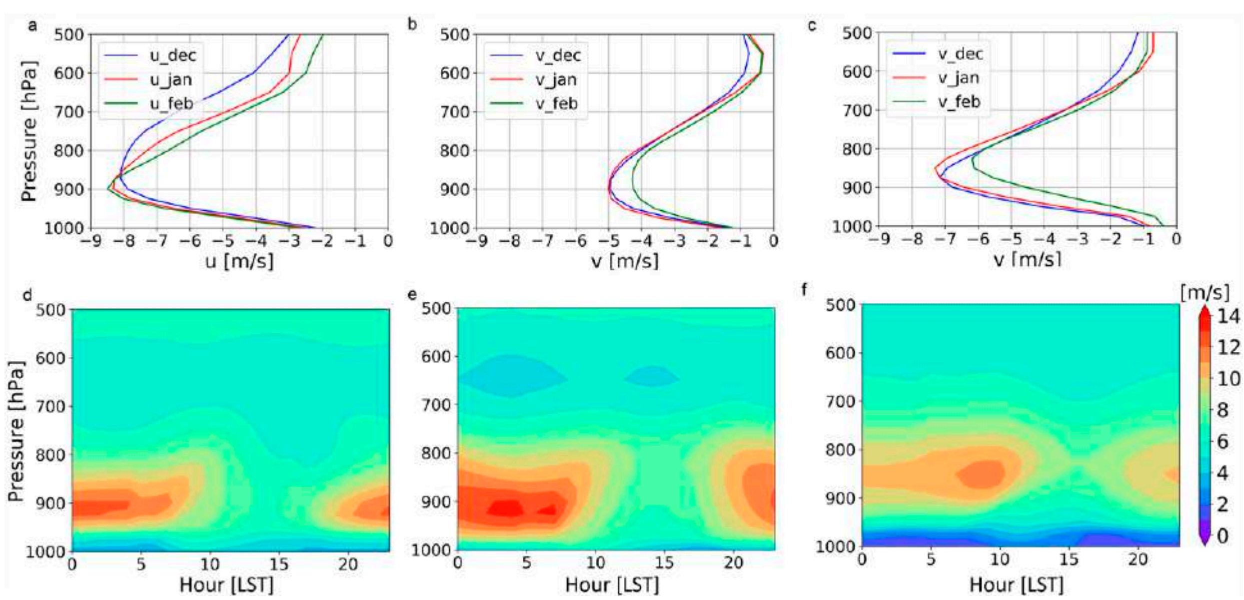

FIG. 5. Monthly mean vertical profiles of (a) zonal winds (m s^{-1}) at the entrance region defined over 6°–10°N and 63°–65°W, (b) meridional winds (m s^{-1}) over the midcorridor at 5°N and 70°–74°W, and (c) meridional winds over the exit region at 1.5°N and 71°–75°W during DJF between 1981 and 2019. Diurnal cycle of wind speeds during DJF 1981–2019 for different cores: (d) C1 (6°–10°N), (e) C2 (7.5°N, 67°W), and (f) C3 (2°N, 73.5°W). The profiles were selected according to Jiménez-Sánchez et al. (2019) and the cores according to Jiménez-Sánchez et al. (2020).

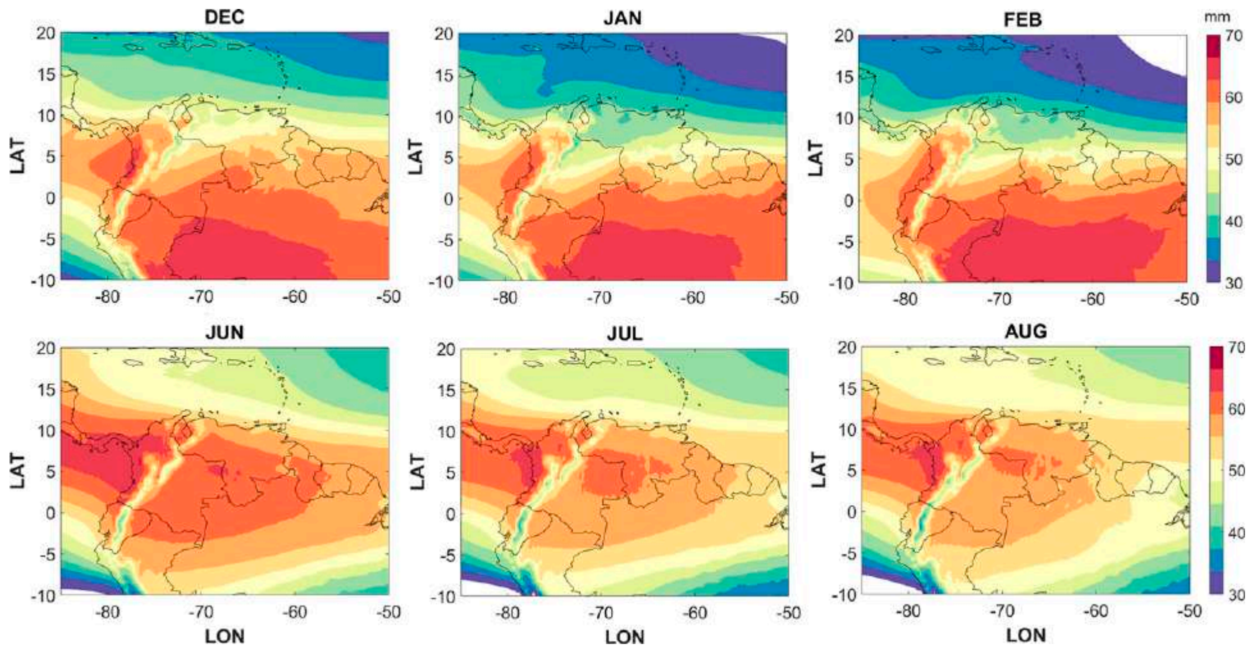

FIG. 6. Long-term mean of total precipitable water (mm) during (top) DJF and (bottom) JJA during the period 1981–2019.

portion over northern Colombia, which is persistent during DJF. Note that implemented criteria can capture nocturnal inland LLJs, such as the OLLJ and the Guiana LLJ (Gimeno et al. 2016). Meanwhile, during JJA, the frequency of occurrence of the OLLJ at 1200 UTC (0700 LST), the hour with the most intense activity, reaches values up to 35% along the OLLJ corridor (Fig. A1 in the appendix).

b. The climatology of precipitation and the OLLJ

Figure 3b shows the annual cycle of precipitation estimated for the Colombian Orinoco region using the precipitation stations and gridded datasets. We only considered precipitation stations in Colombia, although the Orinoco region represents the hydro-ecological basins shared between the Colombian

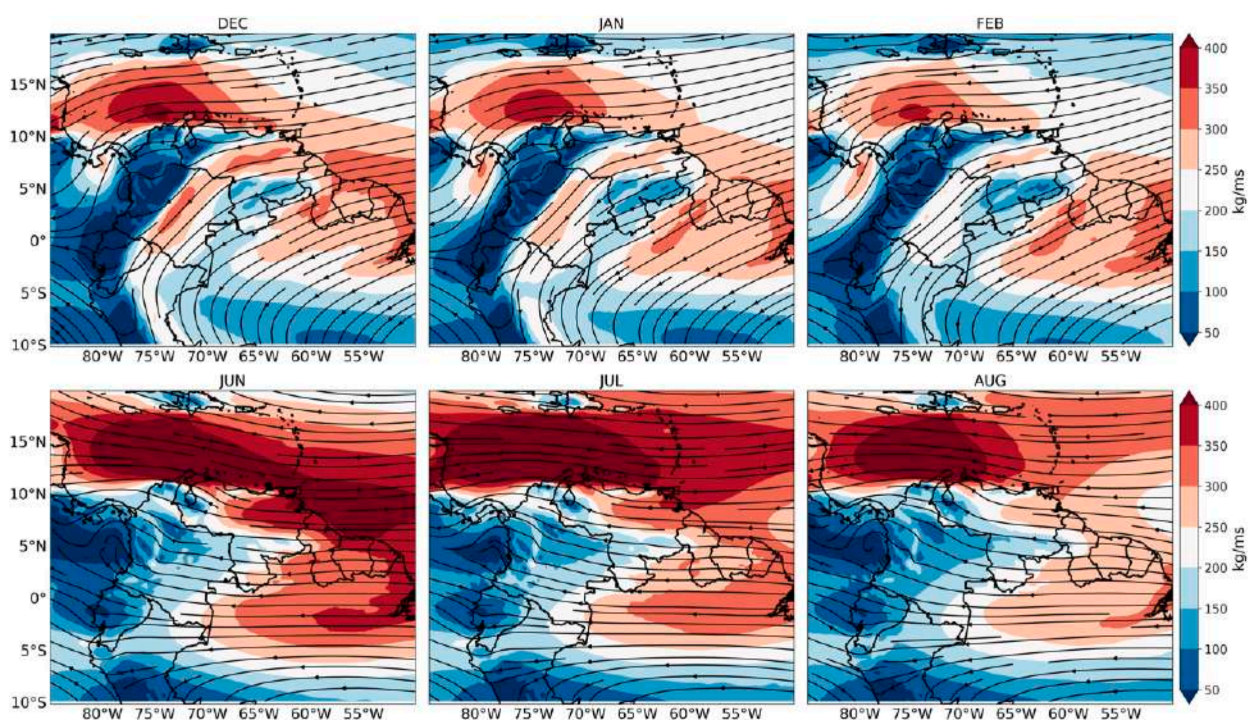

FIG. 7. Long-term mean of vertical integral of water vapor flux (kg m^{-1} s^{-1}) from ERA5 and streamlines for (top) DJF and (bottom) JJA.

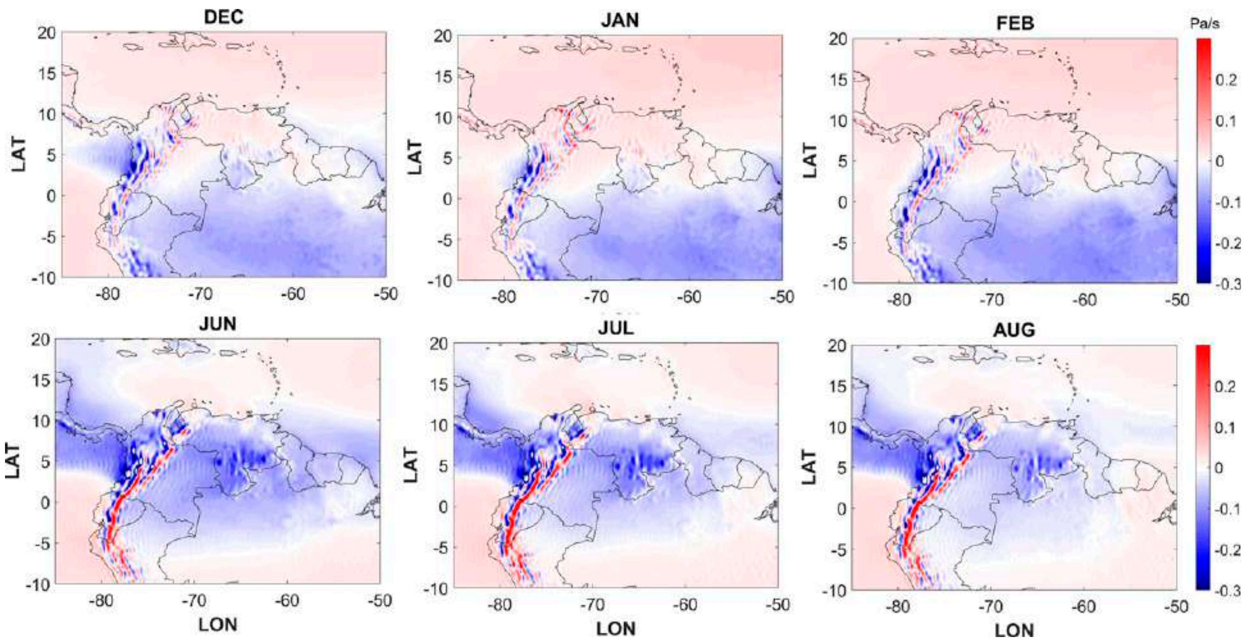

FIG. 8. Long-term mean of omega at 500 hPa (Pa s^{-1}) from ERA5 during DEF and JJA for the period 1981–2019.

eastern Andes and Venezuela. The highest values of precipitation over the region are observed during May–July in all datasets, including those estimated as an ensemble from all stations (gray area in Fig. 3b). In contrast, all datasets show that the dry season occurs during DJF. Gridded datasets (e.g., CHIRPS and GPCC) adequately represent the pattern of the annual cycle shown by the rain gauge stations, with higher differences during the wet season than the dry season. Our results are consistent with LaBar et al. (2005) and Urrea et al. (2019), who show that the lowest daily precipitation

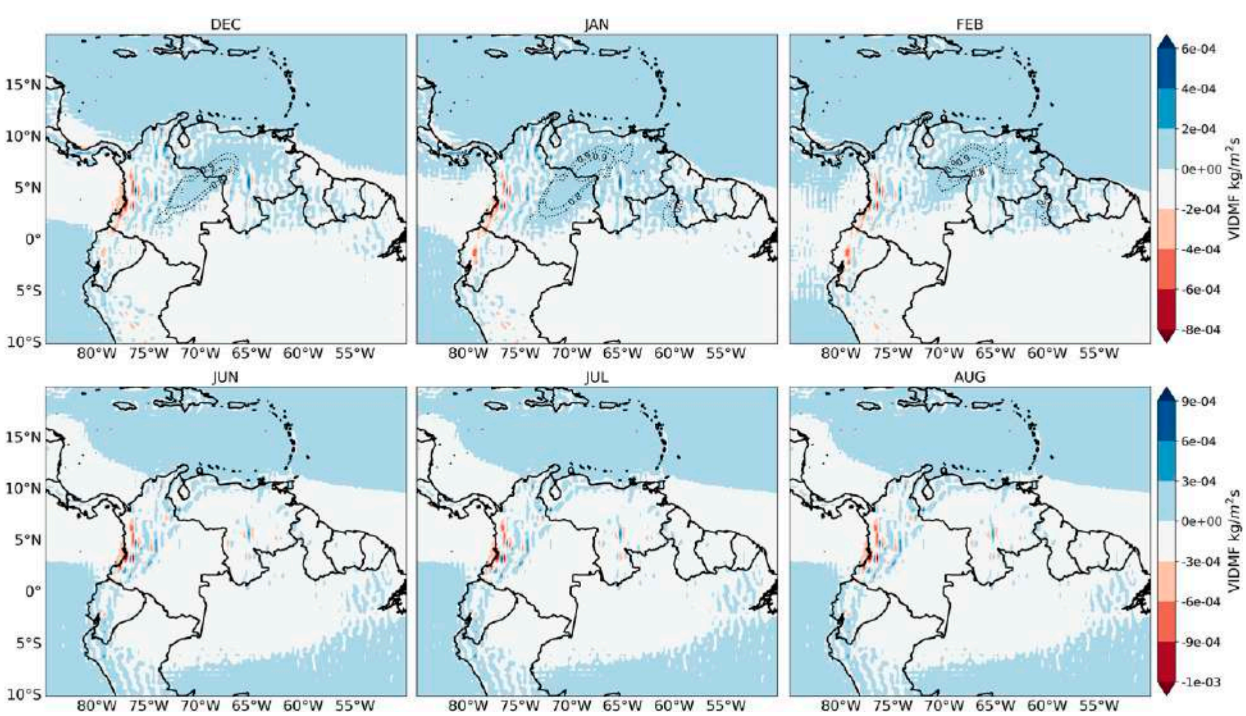

FIG. 9. Long-term mean of vertically integrated moisture divergence flux (kg m^{-2} s^{-1}) from ERA5 for DJF and JJA. Frequencies above 80% of occurrence of an LLJ are shown in contours.

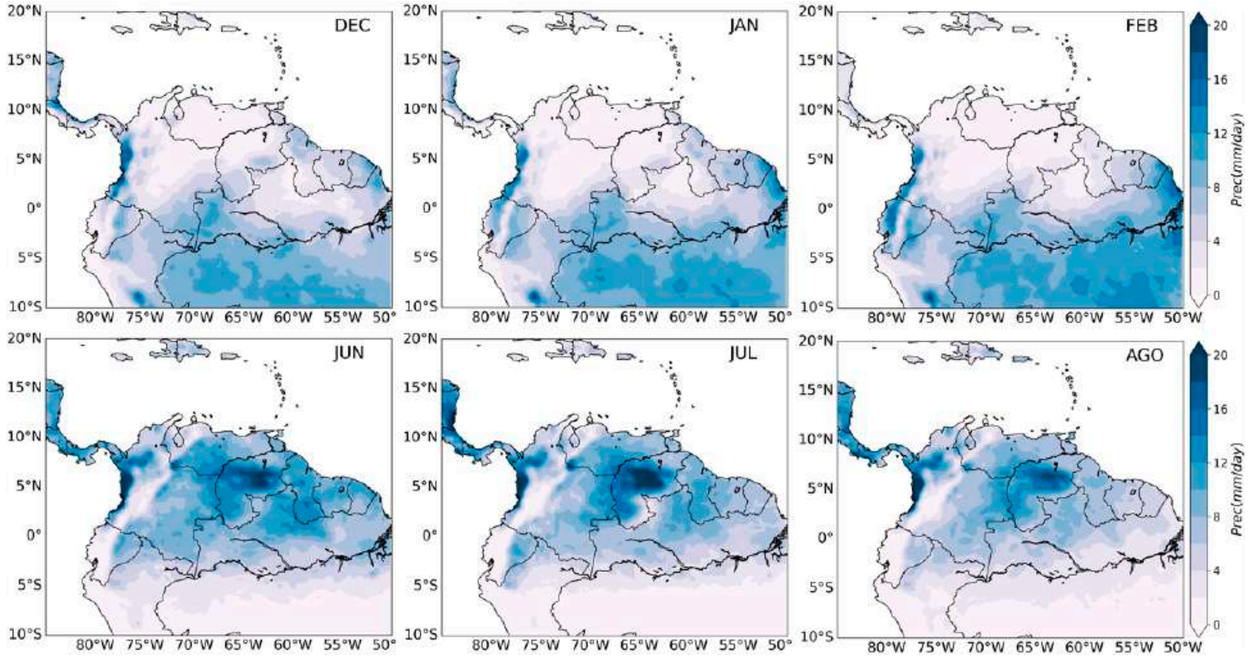

FIG. 10. Composite of precipitation during the season of extreme activity of the OLLJ. (top) Precipitation during DJF for strong zonal winds of the OLLJ. (bottom) Precipitation during JJA for weak winds of the OLLJ.

occurs during DJF over the plains of eastern Colombia and Venezuelan western.

Figure 4 shows the fields of long-term monthly precipitation in northern South America during the months of extreme activity for the OLLJ. During DJF, a band of precipitation around 10 mm day^{-1} is located below the equator (5°S) in the Amazon region. This band is related to the meridional migration of the ITCZ (Berry and Reeder 2014) and the onset of the South American monsoon system (Liebmann and Mechoso 2011). In contrast, during June–August (JJA), the precipitation band is located around 5°N over the Colombia–Venezuela plains (up to 15 mm day^{-1}) and Colombian Pacific (around 20 mm day^{-1}).

Figure 4 also shows the mean fields of wind speed at 925 hPa for DJF and JJA. For DJF, winds are predominantly northeasterlies at the easternmost part of Venezuela related to the OLLJ (Jiménez-Sánchez et al. 2020; Rueda 2014; Torrealba and Amador 2010). The wind speed in the OLLJ corridor exhibits values around 8–10 m s^{-1}, reaching the eastern Colombian Andes and then shifting southward around 70°W, forced by the topographic barrier of the Andes. In contrast, during JJA, the LLJ retreats and decreases in intensity (wind speeds below 5 m s^{-1}; Fig. 3a), and the maximal precipitation rates occur over central Venezuela and eastern Colombia (Fig. 4, bottom).

The monthly mean vertical profiles of the zonal and meridional wind speeds along the OLLJ pathway during DJF are shown in Fig. 5. Based on topographic effects, Jiménez-Sánchez et al. (2020) proposed three regions where the jet develops: entrance, midcorridor, and exit (Fig. 1). Due to the predominant direction of the winds over each region, zonal or meridional winds were selected for the vertical profiles: zonal winds were used over the entrance region profiles, while in midcorridor and exit regions, the profiles are estimated using the meridional winds (Fig. 1). Over the entrance region, maximal zonal wind magnitudes predominate during DJF (around 8–9 m s^{-1}), whereas meridional wind speeds range between 4 and 5 m s^{-1} for the midcorridor and between 6 and 7 m s^{-1} for the exit region. For midcorridor and exit regions, the weakest values occur in February. These peak values are reached at 900 hPa for the entrance and midcorridor; whereas meridional wind speed maxima are located at 850 hPa for the exit region, where SALLJ predominates (Montini et al. 2019). These maximal wind values are in agreement with the annual cycle of wind speeds at the Colombian Orinoco region as shown in Fig. 3a. Figure 5 (bottom) also shows the diurnal cycle of wind speeds. Maximal wind speeds are located from 925 to 900 hPa and occur between midnight and 0400 LST at the entrance and between 0300 and 0700 LST in the midcorridor. At the exit region, the maxima move from 0800 to 1000 LST and are located at 850 hPa. These long-term results agree with the simulations of Jiménez-Sánchez et al. (2020), except that two peaks are found in the midcorridor: one occurring between 0300 and 0500 LST and the other around 0700 LST.

c. *Moisture transport by the OLLJ*

To establish a connection between the OLLJ and precipitation, we examine the TPW, omega, atmospheric water vapor flux, and vertically integrated moisture divergence flux (VIMDF). Figure 6 shows the climatology of TPW during DJF and JJA. Values of the TPW around 70 mm (the highest in the study region) are located over the Amazon and southern Colombia during DJF (exit region of the OLLJ); while in

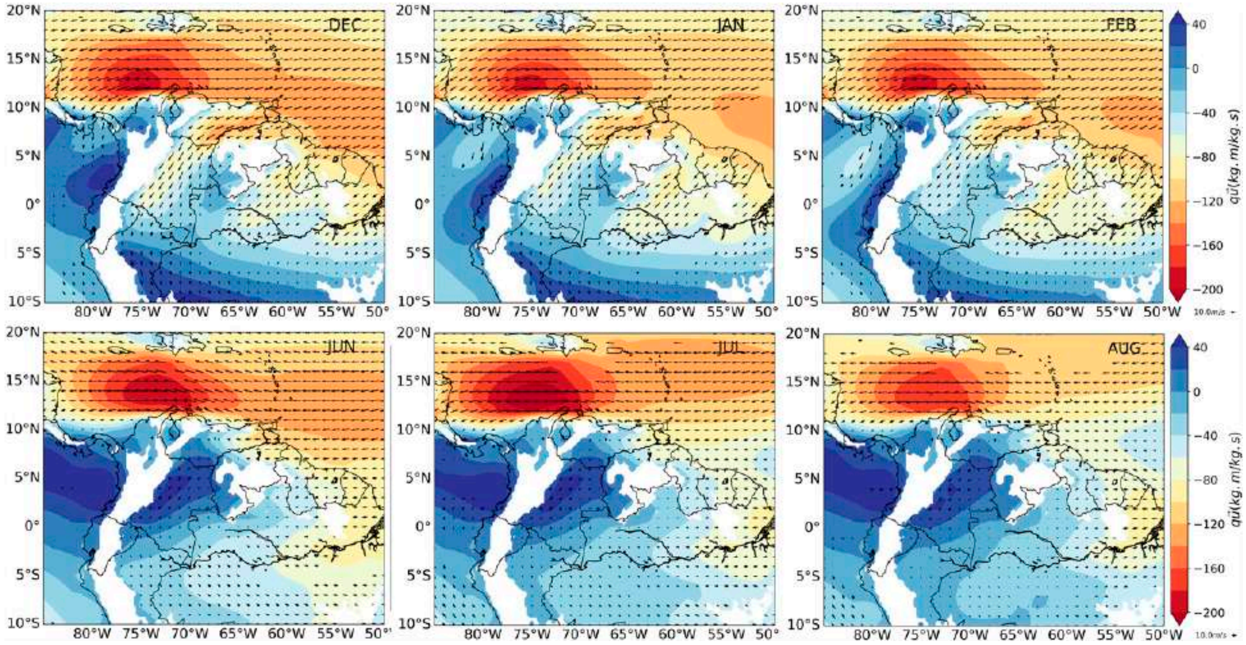

FIG. 11. Composite of zonal water vapor flux ($q\mathbf{u} \times 10^3$; kg m kg^{-1} s^{-1}) at 925 hPa during the season of extreme activity of the OLLJ. (top) Water vapor flux during DJF for strong zonal winds of the OLLJ. (bottom) Water vapor flux during JJA for weak winds of the OLLJ. Total wind vectors are plotted where the composite of zonal water vapor flux and the long-term mean zonal water vapor flux are statistically different at the 5% significance level.

central and northern Venezuela and the eastern Colombian Plains (OLLJ midcorridor), values decrease from 50 to 40 mm during December–February. A band of high values of TPW (>50 mm) moves toward northwestern South America and Central America during JJA. From June to August, the values of the TPW vary from 60 to 50 mm over the

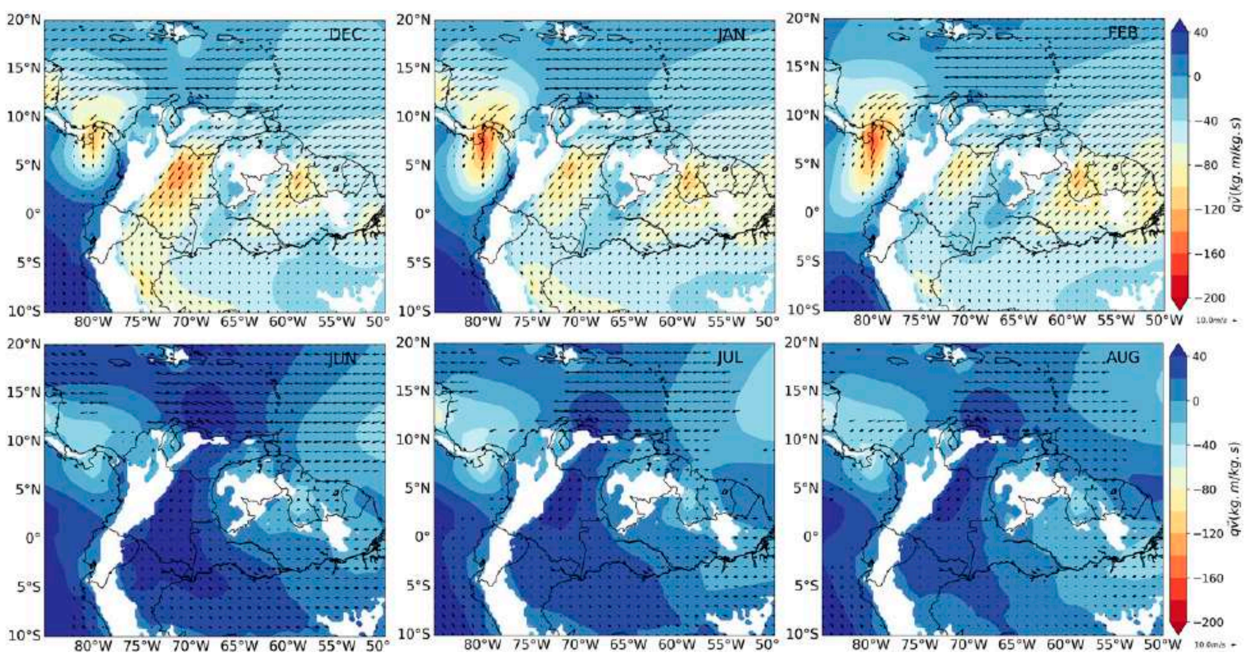

FIG. 12. Composite of meridional water vapor flux ($q\mathbf{v} \times 10^3$; kg m kg^{-1} s^{-1}) at 925 hPa during the season of extreme activity of the OLLJ. (top) Water vapor flux during DJF for strong meridional winds of the OLLJ. (bottom) Water vapor flux during JJA for weak winds of the OLLJ. Total wind vectors are plotted where composite of meridional water vapor flux and the long-term mean meridional water vapor flux are statistically different at the 5% significance level.

Colombian–Venezuelan plains, Guyana, and northwest Brazil. The lowest values of TPW in the study region are located in the OLLJ corridor during the DJF season; during JJA the eastern Pacific and the OLLJ corridor are the regions with the highest values.

The mean fields of monthly vertically integrated water vapor flux (VIWVF) have a region of higher water vapor along the OLLJ corridor for the DJF period (Fig. 7). The long-term monthly mean of VIWVF and its streamlines overlap and show that there are both zonal and meridional pathways of water vapor along the OLLJ corridor during DJF and predominantly zonal moisture transport during JJA. Along the OLLJ and the Guianas LLJ corridors, there are values of the VIWVF from 250 to 350 kg m^{-1} s^{-1} (the highest in northern South America) that are transported from the tropical Atlantic Ocean to the central Venezuela and the Colombian east plains during December and coincide with the moisture sources of those LLJs described by Algarra et al. (2019). The values of VIWVF over the OLLJ corridor decrease from 200 to 300 kg m^{-1} s^{-1} in January to less than 200 kg m^{-1} s^{-1} in February. This reduction of the values of the VIWVF may influence the availability of water at the exit of the OLLJ or the southern regions of the continent.

Unlike with the OLLJ, for the Guianas LLJ, the values of the VIWVF start at 200 kg m^{-1} s^{-1} in December and gradually increase to 350 kg m^{-1} s^{-1} in February, with a similar moisture source and sink as the OLLJ, as also suggested by the results of Algarra et al. (2019). One striking feature is that both the OLLJ and the Guianas LLJ corridors are the two regions with the highest values of VIWVF during the DJF season, becoming the most important pathways for water vapor flux over northern South America. This result is supported by the fact that nearly 80% of the total water vapor flux occurs at low levels (between 1000 and 800 hPa; Fig. A2, top), while 12%–14% of the water vapor at low level is carried out along the OLLJ corridor at 925 hPa during DJF (Fig. A2, bottom).

Despite the reduced values of TPW during DJF (around 45 mm)–in comparison with JJA–there is a water vapor flux of 200–300 kg m^{-1} s^{-1} transported from the northeasterly flow along the OLLJ region in Venezuela and then continuing southward (around 5°N–75°W) forced by topographic effects of the eastern Andean mountain range in Colombia (Fig. 4). However, these moisture transport conditions occur during the dry season over the Orinoco region (and a downward flow, as shown by Fig. 8), as is shown by the monthly mean precipitation during DJF (Figs. 3 and 4). We hypothesize that the strongest winds of the OLLJ favor the transport of moisture in such amounts (Fig. 4), and it might be related to an inhibition of convection as shown by LaBar et al. (2005) and supported by the divergence flux, which coincides with the strongest frequency of occurrence (80%–90%) of the jet over the Orinoco region (Fig. 9).

d. Analysis of extreme OLLJ activity

Figure 10 (top) shows a composite of the precipitation over northern South America during DJF for the key times described in section 3. The composites of precipitation show that during DJF, daily precipitation values are close to 0 mm day^{-1}; except for increased precipitation in the border between Colombia, Ecuador, Peru, and Brazil. In contrast, Fig. 10 (bottom) shows precipitation composites during the period of a low frequency of occurrence of the OLLJ (JJA; Fig. A1), which shows that precipitation increases in the range of 5–10 mm day^{-1} in the OLLJ corridor. Moreover, rainfall composites reveal an increase of precipitation over Venezuela, whose location coincides with the upward flow presented in Fig. 8 and a high TPW zone over Venezuela and the Guianas, presented in Fig. 6. Indeed, a detailed analysis of the time series for the composite indicates that the relative frequencies of daily precipitation with stronger (weaker) events of the OLLJ during DJF (JJA) are less (more) than 20% (70%) along the OLLJ corridor (Fig. A3). During JJA, the OLLJ corridor exhibits the highest relative frequencies of daily precipitation in southeastern Venezuela (up to 70%), while for the Colombian region it reaches the lowest values (around 40%) (Fig. A3). These results confirm the association that a dry (wet) season occurs during stronger (weaker) OLLJ in DJF (JJA). It also provides useful information for rainfall prediction and its applications.

Figure 11 shows the composite for zonal water vapor flux (WVF) at 925 hPa over northern South America. The top row indicates that during DJF, the strongest values of the zonal WVF (greater than 100 kg m kg^{-1} s^{-1}) appear over the CLLJ (tropical North Atlantic Ocean) and OLLJ (Venezuela and Colombian plains) pathways. In contrast, Fig. 11 (bottom) shows composites of zonal WVF during the season of the low frequency of occurrence of the OLLJ (JJA). During this season, the highest values of the zonal WVF come from the tropical North Atlantic Ocean toward the Caribbean Sea bordering the Venezuelan and Colombian coasts.

Figure 12 shows a composite for the meridional WVF during DJF and JJA. During DJF (top row), the OLLJ is an important mechanism of meridional water transport through the Orinoco and Amazon Colombian regions. Note that in the corridor of the OLLJ, the meridional WVF exhibits its strongest activity during December (100 kg m kg^{-1} s^{-1}) and decays during subsequent months (January and February). Moreover, Fig. 12 (top) shows that the 925-hPa northerly cross-equatorial flow (Wang and Fu 2002) are winds that correspond to the OLLJ, which pass toward the Amazon River basin.

Our results evidence an increase of the WVF from the Amazon River basin toward northern South America at 925 hPa during JJA (Fig. 12, bottom) reaching values around 50 kg m kg^{-1} s^{-1}, which are the highest values around the year from this source. This increase in water vapor transport during the JJA in the northward direction is related to the intensification of the southerly cross-equatorial flow (Wang and Fu 2002). In this regard, Paccini et al. (2018) state that the atmospheric circulation pattern that develops during a JJA in the Amazon River basin relates to the cross-equatorial flow and may induce intense precipitation in the Amazon–Andes transition region during a

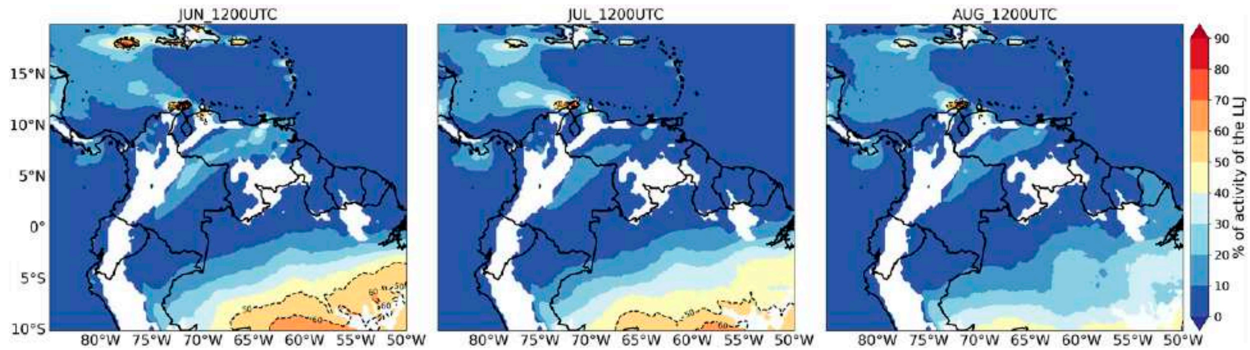

FIG. A1. Monthly percentage of days during the month when the three OLLJ criteria are satisfied during the 1981–2019 period at 1200 UTC (0700 LST).

JJA, which can be related to the higher WVF in the border between Peru and Colombia.

5. Conclusions and future work

The long-term activity of the Orinoco low-level jet (OLLJ) was characterized by the criteria for the frequency of occurrence of a low-level jet (LLJ) reported in the literature and the ERA5 atmospheric reanalysis. Our results evidence the spatiotemporal features of the OLLJ, which is relatively stronger during December–February (DJF) with values around 8–10 m s^{-1}, and its highest frequencies of occurrence are drawn over the plains of Venezuela and eastern Colombia. These criteria for LLJ activity allowed us to verify that the occurrence of the OLLJ exhibits daily frequencies above 80% (below 40%) during DJF [June–August (JJA); Fig. A1]. In this, we extend to the long-term period the findings of Jiménez-Sánchez et al. (2020) who performed a 5-month study. In a regional context, these criteria also identify other inland and coastal wind flows, such as the Guianas LLJ and the Panama Jet.

During DJF, a composite analysis of the extreme activity of the OLLJ showed an increase in precipitation beyond the jet exit region (the Amazon River basin) while there is an enhanced moisture flux over the OLLJ corridor through the plains of Venezuela and eastern Colombian compared to JJA. Hence, these results indicate that OLLJ constitutes a mechanism of moisture flux from the tropical North Atlantic Ocean to the Amazon River basin. During JJA, the jet activity decreases, and the composite analysis shows that precipitation decreases over the Amazon. For this season (JJA), the jet retreats and the moisture transported through the jet pathway

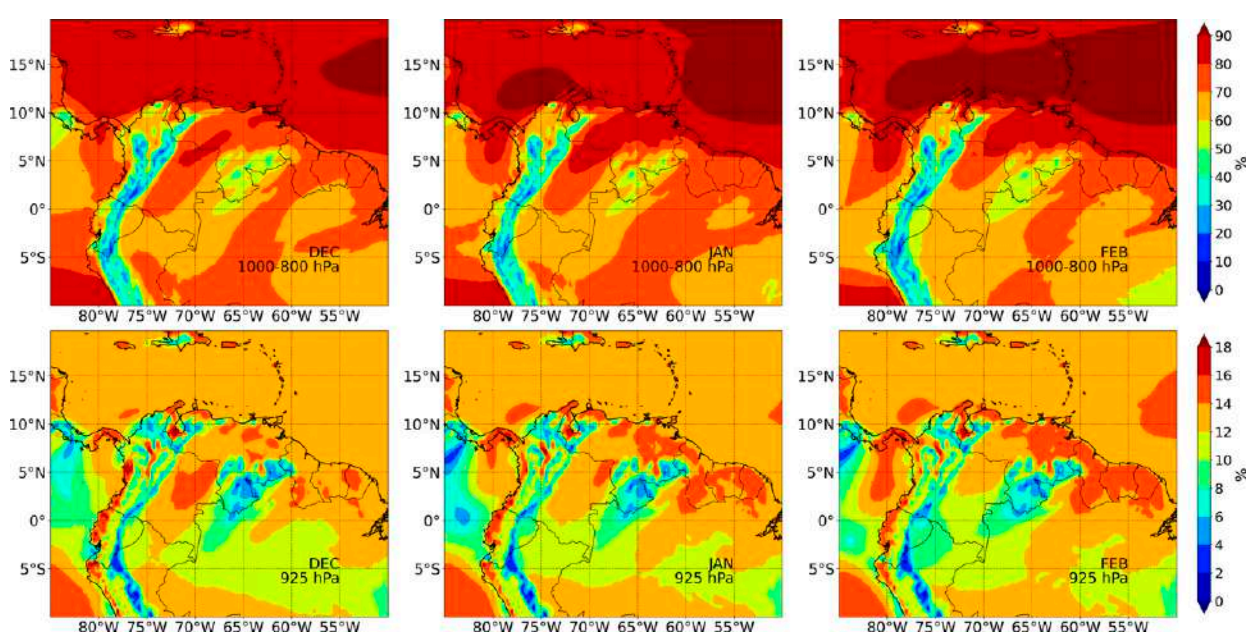

FIG. A2. Percentage of moisture transport during DJF (top) in the 1000–800-hPa layer with respect to the entire atmospheric profile $\left\{\left[q|V|_{1000-800}/\left(q|V|_{\mathrm{ap}}\right)\right]\times 100\right\}$ and (bottom) at 925 hPa with respect to the 1000–800-hPa layer $\left\{\left[q|V|_{925}/\left(q|V|_{1000-800}\right)\right]\times 100\right\}$.

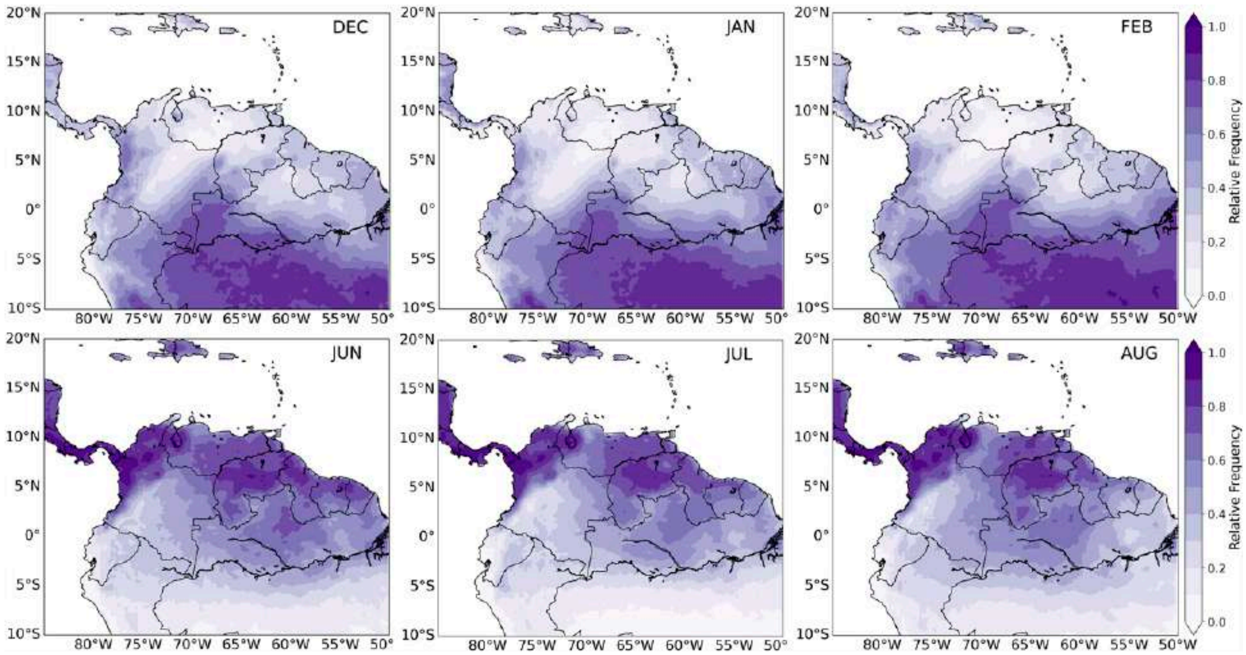

FIG. A3. Relative frequency of daily precipitation during extreme activity of the OLLJ.

to the Amazon basin diminishes. Based on a meridional wind index, Wang and Fu (2002) related the northerly (southerly) flow with the onset (end) of the wet season over the Amazon. In agreement with previous work, our results showed that during JJA, there is an increased southerly water vapor flux (WVF) from the Amazon River basin when the OLLJ reaches its lowest activity. In contrast, during DJF, enhanced values of northerly WVF from the Atlantic Ocean prevail over the corridor. Thus, OLLJ constitutes a mechanism of moisture transport from the tropical North Atlantic Ocean to the Amazon during DJF, whereas the southerly cross-equatorial flow prevails over the Venezuela and Colombia plains during JJA.

Over the Orinoco region, the OLLJ and the precipitation relate in the opposite way. During DJF, the OLLJ shows the highest frequency of occurrence and the dry season predominates. During JJA, the OLLJ reduces its frequency of occurrence, a southerly cross-equatorial flow develops from the Amazon basin (in the opposite direction of the OLLJ), and the wet season over the Orinoco region occurs.

All these mechanisms are partly explained by the southernmost location of the ITZC (Berry and Reeder 2014), which allows the entrance of the northeasterlies over the northeastern part of South America during DJF. This large amount of atmospheric moisture over the pathway of the OLLJ contributes to the rainy season over northern Peru, Ecuador, northern Brazil, and southern Colombia (the exit region of the OLLJ corridor). During JJA, the ITZC has moved over the Orinoco region (Berry and Reeder 2014; Asmerom et al. 2020; Grodsky and Carton 2003) and the low pressure prevents the entrance of the northeasterlies, and consequently weakens the OLLJ. These results highlight the role of the OLLJ as a mechanism that helps to explain the annual cycle of precipitation over both the Orinoco and Amazon River basin regions.

This study used the ERA5 reanalysis to characterize the diurnal and annual cycle of the OLLJ. Moreover, regarding the OLLJ, there are still questions to be answered in future work, such as

1) How does ENSO influence the dynamics of the OLLJ?
2) What is the interaction between the OLLJ and the SALLJ, and their influence on precipitation in the region?
3) How can we use the OLLJ index to improve the prediction of rainfall and streamflows in the zone of influence of the OLLJ?

These questions draw on some of the topics for further research associated with the OLLJ.

Acknowledgments. A. Builes-Jaramillo was supported by the Institución Universitaria Colegio Mayor de Antioquia. H. D. Salas was supported by the Institución Universitaria Colegio Mayor de Antioquia and by COLCIENCIAS Grant for National Doctorates 617-2. J. Yepes was supported by the project "El Chorro de los Andes Orientales (CHAO) y su relación con la hidro-climatología de Colombia." The authors thank the two anonymous reviewers for their insightful comments and the corrections that improved the outcome of the present study.

Data availability statement. ERA5 Reanalysis data is available at the European Copernicus Programme website (https://www.copernicus.eu/). The CHIRPS precipitation dataset is available at the University of California, Santa Barbara, Climate Hazards Center website (https://www.chc.ucsb.edu/data). The GPCC precipitation dataset is available at the NOAA Physical Sciences

Laboratory website (https://psl.noaa.gov/data/gridded/data.gpcc.html). The rain gauge datasets from Colombia are available at the Colombian Institute for Environmental Studies website (http://dhime.ideam.gov.co).

APPENDIX

Climatological Features over the OLLJ Region

The appendix shows climatologies of the OLLJ frequency of occurrence during JJA (Fig. A1), percentages of moisture transport in the lower atmosphere during DJF (Fig. A2), and the relative frequency of daily precipitation during DJF and JJA (Fig. A3).

REFERENCES

Algarra, I., J. Eiras-Barca, R. Nieto, and L. Gimeno, 2019: Global climatology of nocturnal low-level jets and associated moisture sources and sinks. *Atmos. Res.*, **229**, 39–59, https://doi.org/10.1016/j.atmosres.2019.06.016.

Amador, J. A., 1999: A climate feature of the tropical Americas: The trade wind easterly jet. *Topicos Meteor. Oceanogr.*, **5** (2), 91–102.

Arias, P. A., J. A. Martínez, and S. C. Vieira, 2015: Moisture sources to the 2010–2012 anomalous wet season in northern South America. *Climate Dyn.*, **45**, 2861–2884, https://doi.org/10.1007/s00382-015-2511-7.

Asmerom, Y., and Coauthors, 2020: Intertropical convergence zone variability in the Neotropics during the Common Era. *Sci. Adv.*, **6**, eaax3644, https://doi.org/10.1126/sciadv.aax3644.

Berry, G., and M. J. Reeder, 2014: Objective identification of the intertropical convergence zone: Climatology and trends from the ERA-Interim. *J. Climate*, **27**, 1894–1909, https://doi.org/10.1175/JCLI-D-13-00339.1.

Bonner, W. D., 1968: Climatology of the low level jet. *Mon. Wea. Rev.*, **96**, 833–850, https://doi.org/10.1175/1520-0493(1968)096<0833:COTLLJ>2.0.CO;2.

Boschat, G., I. Simmonds, A. Purich, T. Cowan, and A. B. Pezza, 2016: On the use of composite analyses to form physical hypotheses: An example from heat wave–SST associations. *Sci. Rep.*, **6**, 29599, https://doi.org/10.1038/srep29599.

Brook, R. R., 1985: The Koorin nocturnal low-level jet. *Bound.-Layer Meteor.*, **32**, 133–154, https://doi.org/10.1007/BF00120932.

Douglas, M. W., 1995: The summertime low-level jet over the Gulf of California. *Mon. Wea. Rev.*, **123**, 2334–2347, https://doi.org/10.1175/1520-0493(1995)123<2334:TSLLJO>2.0.CO;2.

Findlater, J., 1969: A major low-level air current near the Indian Ocean during the northern summer. *Quart. J. Roy. Meteor. Soc.*, **95**, 362–380, https://doi.org/10.1002/qj.49709540409.

Funk, C., and Coauthors, 2015: The climate hazards infrared precipitation with stations–A new environmental record for monitoring extremes. *Sci. Data*, **2**, 21, https://doi.org/10.1038/sdata.2015.66.

Gimeno, L., and Coauthors, 2016: Major mechanisms of atmospheric moisture transport and their role in extreme precipitation events. *Annu. Rev. Environ. Resour.*, **41**, 117–141, https://doi.org/10.1146/annurev-environ-110615-085558.

Grodsky, S. A., and J. A. Carton, 2003: The intertropical convergence zone in the South Atlantic and the equatorial cold tongue. *J. Climate*, **16**, 723–733, https://doi.org/10.1175/1520-0442(2003)016<0723:TICZIT>2.0.CO;2.

Hersbach, H., and Coauthors, 2019: Global reanalysis: Goodbye ERA-Interim, hello ERA5. *ECMWF Newsletter*, No. 159, ECMWF, Reading, United Kingdom, 17–24, https://www.ecmwf.int/node/19027.

Jiménez-Sánchez, G., P. M. Markowski, V. Jewtoukoff, G. S. Young, and D. J. Stensrud, 2019: The Orinoco low-level jet: An investigation of its characteristics and evolution using the WRF model. *J. Geophys. Res. Atmos.*, **124**, 10 696–10 711, https://doi.org/10.1029/2019JD030934.

——, ——, G. S. Young, and D. J. Stensrud, 2020: The Orinoco low-level jet: An investigation of its mechanisms of formation using the WRF model. *J. Geophys. Res. Atmos.*, **125**, e2020JD032810, https://doi.org/10.1029/2020JD032810.

Kinuthia, J., and G. Asnani, 1982: A newly found jet in North Kenya (Turkana Channel). *Mon. Wea. Rev.*, **110**, 1722–1728, https://doi.org/10.1175/1520-0493(1982)110<1722:ANFJIN>2.0.CO;2.

LaBar, R. J., M. Douglas, J. Murillo, and J. F. Mejia, 2005: The Llanos low-level jet and its association with Venezuelan convective precipitation. Tech. Rep., 21 pp., http://www.caps.ou.edu/reu/reu05/finalpapers/LaBar-finalpaper.pdf.

Liebmann, B., and C. R. Mechoso, 2011: The South American monsoon system. *The Global Monsoon System: Research and Forecast*. World Scientific, 137–157, https://doi.org/10.1142/9789814343411_0009.

Martin, E. R., and C. Schumacher, 2011: The Caribbean low-level jet and its relationship with precipitation in IPCC AR4 models. *J. Climate*, **24**, 5935–5950, https://doi.org/10.1175/JCLI-D-11-00134.1.

Montini, T. L., C. Jones, and L. M. Carvalho, 2019: The South American low-level jet: A new climatology, variability, and changes. *J. Geophys. Res. Atmos.*, **124**, 1200–1218, https://doi.org/10.1029/2018JD029634.

Montoya, G., J. Pelkowski, and J. Eslava, 2001: Sobre los vientos alisios del nordeste y la existencia de una corriente en el piedemonte oriental andino. *Rev. Acad. Colomb. Cienc. Exactas Fis. Nat.*, **25**, 363–370.

Morales, J., P. Arias, and J. Martínez, 2017: Role of Caribbean low-level jet and Choco jet in the transport of moisture patterns towards Central America. *First Int. Electronic Conf. on the Hydrological Cycle*, Online, MDPI, 12 pp., https://doi.org/10.3390/CHyCle-2017-04861.

Muñoz, E., A. J. Busalacchi, and A. Ruiz-Barradas, 2008: Winter and summer structure of the Caribbean low-level jet. *J. Climate*, **21**, 1260–1276, https://doi.org/10.1175/2007JCLI1855.1.

Paccini, L., J. C. Espinoza, J. Ronchail, and H. Segura, 2018: Intra-seasonal rainfall variability in the Amazon basin related to large-scale circulation patterns: A focus on western Amazon–Andes transition region. *Int. J. Climatol.*, **38**, 2386–2399, https://doi.org/10.1002/joc.5341.

Peixoto, J., and A. Oort, 1993: *Physics of Climate*. U.S. Department of Energy Office of Scientific and Technical Information, 520 pp.

Poveda, G., and O. J. Mesa, 2000: On the existence of Lloró (the rainiest locality on Earth): Enhanced ocean–land–atmosphere interaction by a low-level jet. *Geophys. Res. Lett.*, **27**, 1675–1678, https://doi.org/10.1029/1999GL006091.

Ranjha, R., G. Svensson, M. Tjernström, and A. Semedo, 2013: Global distribution and seasonal variability of coastal low-level jets derived from ERA-Interim reanalysis. *Tellus*, **65A**, 20412, https://doi.org/10.3402/tellusa.v65i0.20412.

Rife, D. L., J. O. Pinto, A. J. Monaghan, C. A. Davis, and J. R. Hannan, 2010: Global distribution and characteristics of diurnally varying low-level jets. *J. Climate*, **23**, 5041–5064, https://doi.org/10.1175/2010JCLI3514.1.

Rodríguez-Gómez, C., G. Echeverry, A. Jaramillo, and L. A. Ladino, 2022: The negative impact of biomass burning and the Orinoco low-level jet on the air quality of the Orinoco River Basin. *Atmósfera*, https://doi.org/10.20937/ATM.52979, in press.

Rueda, C., 2014: Caracterización de la Corriente en Chorro de Bajo Nivel de los Llanos Orientales Colombianos. M.Sc. thesis, Dept. de Geociencias, Universidad Nacional de Colombia, 84 pp.

Schneider, U., A. Becker, P. Finger, A. Meyer-Christoffer, M. Ziese, and B. Rudolf, 2014: GPCC's new land surface precipitation climatology based on quality-controlled in situ data and its role in quantifying the global water cycle. *Theor. Appl. Climatol.*, **115**, 15–40, https://doi.org/10.1007/s00704-013-0860-x.

Stensrud, D. J., 1996: Importance of low-level jets to climate: A review. *J. Climate*, **9**, 1698–1711, https://doi.org/10.1175/1520-0442(1996)009<1698:IOLLJT>2.0.CO;2.

Terray, P., P. Delecluse, S. Labattu, and L. Terray, 2003: Sea surface temperature associations with the late Indian summer monsoon. *Climate Dyn.*, **21**, 593–618, https://doi.org/10.1007/s00382-003-0354-0.

Torrealba, E. R., and J. A. Amador, 2010: La corriente en chorro de bajo nivel sobre los Llanos Venezolanos de Sur América. *Rev. Climatol.*, **10**, 1–20.

Urrea, V., A. Ochoa, and O. Mesa, 2019: Seasonality of rainfall in Colombia. *Water Resour. Res.*, **55**, 4149–4162, https://doi.org/10.1029/2018WR023316.

Vera, C., and Coauthors, 2006: The South American low-level jet experiment. *Bull. Amer. Meteor. Soc.*, **87**, 63–78, https://doi.org/10.1175/BAMS-87-1-63.

Walters, C. K., J. A. Winkler, S. Husseini, R. Keeling, J. Nikolic, and S. Zhong, 2014: Low-level jets in the North American Regional Reanalysis (NARR): A comparison with rawinsonde observations. *J. Appl. Meteor. Climatol.*, **53**, 2093–2113, https://doi.org/10.1175/JAMC-D-13-0364.1.

Wang, C., 2007: Variability of the Caribbean low-level jet and its relations to climate. *Climate Dyn.*, **29**, 411–422, https://doi.org/10.1007/s00382-007-0243-z.

Wang, H., and R. Fu, 2002: Cross-equatorial flow and seasonal cycle of precipitation over South America. *J. Climate*, **15**, 1591–1608, https://doi.org/10.1175/1520-0442(2002)015<1591:CEFASC>2.0.CO;2.

Whiteman, C. D., X. Bian, and S. Zhong, 1997: Low-level jet climatology from enhanced rawinsonde observations at a site in the southern Great Plains. *J. Appl. Meteor.*, **36**, 1363–1376, https://doi.org/10.1175/1520-0450(1997)036<1363:LLJCFE>2.0.CO;2.

Whyte, F. S., M. A. Taylor, T. S. Stephenson, and J. D. Campbell, 2008: Features of the Caribbean low level jet. *Int. J. Climatol.*, **28**, 119–128, https://doi.org/10.1002/joc.1510.

Xie, S.-P., H. Xu, W. S. Kessler, M. Nonaka, S.-P. Xie, H. Xu, W. S. Kessler, and M. Nonaka, 2005: Air–sea interaction over the eastern Pacific warm pool: Gap winds, thermocline dome, and atmospheric convection. *J. Climate*, **18**, 5–20, https://doi.org/10.1175/JCLI-3249.1.

Xie, Z., A. Duan, and Q. Tian, 2017: Weighted composite analysis and its application: An example using ENSO and geopotential height. *Atmos. Sci. Lett.*, **18**, 435–440, https://doi.org/10.1002/asl.786.

Yepes, J., G. Poveda, J. F. Mejía, L. Moreno, and C. Rueda, 2019: CHOCO-JEX: A research experiment focused on the Chocó low-level jet over the far eastern Pacific and western Colombia. *Bull. Amer. Meteor. Soc.*, **100**, 779–796, https://doi.org/10.1175/BAMS-D-18-0045.1.

No.	NOMBRE	ISSN	CATEGORIA	VIGENCIA	LISTA_SIR
5097	MOLECULAR THERAPY	1525-0016; 1525-0024	A1	Enero 2021 - Diciembre 2021	Scimago Journal Rank - SJR; Journal Citation Reports - JCR
5098	JOURNAL OF MOLECULAR DIAGNOSTICS	1525-1578; 1943-7811	A1	Enero 2021 - Diciembre 2021	Scimago Journal Rank - SJR; Journal Citation Reports - JCR
5099	GEOCHEMISTRY GEOPHYSICS GEOSYSTEMS	1525-2027	A1	Enero 2021 - Diciembre 2021	Scimago Journal Rank - SJR; Journal Citation Reports - JCR
5100	MULTINATIONAL BUSINESS REVIEW	1525-383X; 2054-1686	A1	Enero 2021 - Diciembre 2021	Scimago Journal Rank - SJR; Journal Citation Reports - JCR
5101	JAIDS JOURNAL OF ACQUIRED IMMUNE DEFICIENCY SYNDROMES	1525-4135; 1944-7884	A1	Enero 2021 - Diciembre 2021	Index Medicus; Scimago Journal Rank - SJR; Journal Citation Reports - JCR
5102	FOOD REVIEWS INTERNATIONAL	1525-6103; 8755-9129	A1	Enero 2021 - Diciembre 2021	Scimago Journal Rank - SJR; Journal Citation Reports - JCR
5103	LEVIATHAN	1525-6995; 1750-1849	A1	Enero 2021 - Diciembre 2021	Arts and Humanities Citation Index (AHCI); Scimago Journal Rank - SJR
5104	CLINICAL LUNG CANCER	1525-7304; 1938-0690	A1	Enero 2021 - Diciembre 2021	Scimago Journal Rank - SJR; Journal Citation Reports - JCR
5105	COMMUNICATION DISORDERS QUARTERLY	1525-7401; 1538-4837	A1	Enero 2021 - Diciembre 2021	PsycINFO; Scimago Journal Rank - SJR; Journal Citation Reports - JCR
5106	JOURNAL OF HYDROMETEOROLOGY	1525-7541; 1525-755X	A1	Enero 2021 - Diciembre 2021	Scimago Journal Rank - SJR; Journal Citation Reports - JCR
5107	BIOMACROMOLECULES	1525-7797; 1526-4602	A1	Enero 2021 - Diciembre 2021	Scimago Journal Rank - SJR; Journal Citation Reports - JCR
5108	FIELD METHODS	1525-822X; 1552-3969	A1	Enero 2021 - Diciembre 2021	PsycINFO; Scimago Journal Rank - SJR; Journal Citation Reports - JCR
5109	JOURNAL OF THE AMERICAN MEDICAL DIRECTORS ASSOCIATION	1525-8610; 1538-9375	A1	Enero 2021 - Diciembre 2021	Scimago Journal Rank - SJR; Journal Citation Reports - JCR
5110	PAEDIATRIC RESPIRATORY REVIEWS	1526-0542; 1526-0550	A1	Enero 2021 - Diciembre 2021	Scimago Journal Rank - SJR; Journal Citation Reports - JCR
5111	PAIN MEDICINE	1526-2375; 1526-4637	A1	Enero 2021 - Diciembre 2021	PsycINFO; Scimago Journal Rank - SJR; Journal Citation Reports - JCR
5112	GLOBAL ENVIRONMENTAL POLITICS	1526-3800; 1536-0091	A1	Enero 2021 - Diciembre 2021	Scimago Journal Rank - SJR; Journal Citation Reports - JCR
5113	INTERNATIONAL JOURNAL OF SPORT NUTRITION AND EXERCISE METABOLISM	1526-484X; 1543-2742	A1	Enero 2021 - Diciembre 2021	Scimago Journal Rank - SJR; Journal Citation Reports - JCR
5114	PEST MANAGEMENT SCIENCE	1526-498X	A1	Enero 2021 - Diciembre 2021	Scimago Journal Rank - SJR; Journal Citation Reports - JCR
5115	AMERICAN JOURNAL OF BIOETHICS	1526-5161; 1536-0075	A1	Enero 2021 - Diciembre 2021	Scimago Journal Rank - SJR; Journal Citation Reports - JCR
5116	JOURNAL OF PAIN	1526-5900; 1528-8447	A1	Enero 2021 - Diciembre 2021	PsycINFO; Scimago Journal Rank - SJR; Journal Citation Reports - JCR
5117	JOURNAL OF ENDOVASCULAR THERAPY	1526-6028; 1545-1550	A1	Enero 2021 - Diciembre 2021	Scimago Journal Rank - SJR; Journal Citation Reports - JCR
5118	JOURNAL OF MANUFACTURING PROCESSES	1526-6125	A1	Enero 2021 - Diciembre 2021	Scimago Journal Rank - SJR; Journal Citation Reports - JCR